IEEE Access
Multidisciplinary | Rapid Review | Open Access Journal

Received May 7, 2021, accepted May 18, 2021, date of publication May 25, 2021, date of current version June 14, 2021.

Digital Object Identifier 10.1109/ACCESS.2021.3083493

An Underwater Integrated Navigation Algorithm to Deal With DVL Malfunctions Based on Deep Learning

DING LI, JIANGNING XU, HONGYANG HE, AND MIAO WU
Department of Navigation Engineering, Naval University of Engineering, Wuhan 430033, China
Corresponding author: Hongyang He (xgdhehongyang@163.com)

This work was supported in part by the National Natural Science Foundation of China under Grant 41804076 and Grant 42004067, and in part by the Natural Science Foundation of Hubei Province under Grant 2018CFB544.

ABSTRACT In underwater navigation systems, Global Navigation Satellite System (GNSS) information cannot be used for navigation. The mainstream method of autonomous underwater vehicles (AUV) underwater navigation system is Doppler Velocity Log (DVL) aided strapdown inertial navigation system (SINS). However, because the DVL is an instrument based on Doppler frequency shift to measure velocity, it is easily affected by the external environment. In a complex underwater environment, DVL output is easily polluted by outliers or even interrupted. In this paper, A new integrated navigation algorithm based on deep learning model is proposed to deal with DVL malfunctions. First, use RKF based on Mahalanobis distance algorithm to eliminate outliers, and then train the Nonlinear AutoRegressive with eXogenous input (NARX) model when DVL is available. When DVL is interrupted, use the NARX model to predict the output of DVL and continue integrated navigation. The proposed NARX-RKF scheme's effectiveness verification was performed on the data set collected by the SINS/DVL ship-mounted experimental system. For comparison, different methods are also compared in the experiment. Experimental results show that NARX-RKF can effectively predict the output of DVL and is significantly better than other methods.

INDEX TERMS Strapdown inertial navigation system, DVL, integrated navigation, deep learning, NARX.

I. INTRODUCTION

High-precision, high-reliability underwater navigation and positioning technology have vital in autonomous underwater vehicles (AUV). It is also a critical technology of the underwater Position, Navigation, and Timing (PNT) system [1]. Underwater navigation and positioning technology are different from land and air navigation and positioning systems. Because the electromagnetic wave signal attenuates severely after passing through the water medium, radio navigation methods such as Global Navigation Satellite System (GNSS) cannot be used for underwater navigation and positioning. Therefore, the Strapdown Inertial Navigation System (SINS), a navigation instrument that does not rely on the outside world, is the main navigation system of AUV [2]. However, since the essence of SINS is an integral calculation system based on Newton's second law, errors will accumulate over time. In order to solve the accuracy problem of underwater navigation and positioning technology, other underwater navigation methods are commonly used to assist SINS. Common auxiliary navigation methods include geophysical navigation [3]–[5]and acoustic navigation [6]–[8]. The research on geophysical navigation is still in its infancy and cannot meet actual needs. On the other hand, underwater positioning systems combining SINS and underwater acoustic systems have been extensively studied, such as integrated navigation system based on doppler velocity log (DVL) aided SINS [7]. SINS and external observation navigation information can be fused to improve positioning accuracy through information fusion technology. Traditional information fusion has Kalman filter (KF) [9], extended Kalman filter (EKF) [10] and other variants based on Kalman filter. However, the DVL is active sonar, so the outputs of DVL will also be disturbed by the external environment. The marine environment is very complicated [11], such as ocean current interference, seabed geological environment, fish school effects, etc. The complex marine environment will cause outliers or even interruptions in the output of DVL [12].

The associate editor coordinating the review of this manuscript and approving it for publication was Wenjie Feng.

When the navigation sensor is interrupted, if only measures to isolate the failed sensor are used, the INS solution error will accumulate over time, and the navigation accuracy will drop rapidly. Therefore, research on navigation sensor interrupt processing methods is of great significance to ensure AUV navigation accuracy.

There are currently two main ideas for the strategies used to deal with the short-term failure or interruption of navigation sensors: One is to implement replacement when a failure occurs through hardware redundancy [13]. The other is to design software redundancy based on mathematical models and use mathematical models to directly replace filters to provide correction information or replace failed sensors to provide measurement information during the interruption period.

The hardware redundancy method can handle short-term failures and handle longer-term failures but requires higher hardware costs and increases the system's complexity. At the same time, it is not conducive to the miniaturization of AUV.

Therefore, for sensor failures, software redundancy methods based on mathematical models are more favored. With the development of artificial intelligence technology, artificial neural networks (ANN) [14], support vector regression (SVR) [15], extreme learning machine (ELM) [16], wavelet neural networks (WNN) [17], random forest regression (RFR) [18], ensemble learning [19] and other artificial intelligence technologies [20] have been verified and applied in the field of navigation, integrated navigation errors are suppressed when the observations are rejected. The research in [20] used the adaptive neuro-fuzzy inference system (ANFIS) to predict the attitude error to reduce the slow convergence of the heading estimation in the traditional initial alignment Kalman filter. Reference [14] attempts to use ANN to completely replace geometric algorithms, that is, to use ANN-based inertial measurement algorithms to directly generate motion states from IMU data. Although it can fundamentally eliminate errors caused by integration, it also loses the important advantages of inertial navigation: short-term accuracy and reliability. None of the above studies considered that the inertial navigation system error is accumulated over time, so a deep learning model based on time series can be considered. Recurrent Neural Network (RNN) is a time series prediction network. Dai *et al*. [21] used RNN to estimate the inertial navigation error when GPS refused in ship navigation. However, most of the ships in this study are in a state of direct sailing at a constant velocity, so the effect of the model in other scenarios is unknown. Li *et al*. [22] used the Nonlinear AutoRegressive with eXogenous input (NARX) model to predict the DVL failure navigation output during the SINS/DVL integrated navigation, but this network only selected the velocity increment as the network input, which did not allow the NARX model to learn the SINS error law well, so the long-term error still increases rapidly when DVL is interrupted.

In order to overcome the outliers in the observation values, several robust Kalman filter methods have been suggested in the literature [23]–[31]. The median-based filter proposed by Chang and Wu [23] can make KF robust, but because it is implemented in a block-based batch processing method, its efficiency is not high and the real-time performance is not good. Boncelet *et al*. constructed KF as a linear regression problem and improved its robustness through M-estimation estimation [25]. However, since observations containing outliers are excluded in this method, the number of other observations should not be less than the state's dimension [27]. This has certain limitations in practical applications. Chang proposed a robust KF method that uses the chi-square test to detect outliers in observations, which can better eliminate outliers [28]. we will use this method to make Kalman filtering robust.

This paper focuses on a SINS/DVL integrated navigation algorithm based on NARX and RKF. RKF based on Mahalanobis distance can eliminate outliers' pollution caused by the complex underwater environment. Use the output when the DVL observation is valid to train the NARX model, predict the output of the DVL when the DVL fails, and perform integrated navigation. The experimental results show that the method proposed in this paper can effectively suppress the pollution of outliers and effectively perform integrated navigation when DVL fails. Moreover, compared with other algorithms, this algorithm has better performance.

This paper's organization structure is as follows: Section 2 construct the state equation and filtering model of the integrated navigation system. In Section 3, the robust Kalman filter based on Mahalanobis distance algorithm are derived. In Section 4, the integrated navigation model optimized by deep learning are derived. Section 5 use ship-mounted experimental data to verify the proposed method. Finally, Section 6 summarizes the proposed method and its performance.

II. AUV INTEGRATED NAVIGATION SYSTEM MODEL

The following co-ordinate frames are used in the paper: denote by n the navigation frame, an orthogonal reference with east-north-up (ENU) geodetic axes, by n' the calculating frame, by i the inertially non-rotating frame, by b the SINS body frame, by e the earth frame [2].

The framework of SINS/DVL integrated navigation as shown in Fig. 1 SINS/DVL integrated navigation have two structures: open-loop and closed-loop [4]. (a) shows the open-loop integrated navigation structure. SINS solution the attitude, velocity and position of the carrier in real-time. Simultaneously, the difference between the velocity measured by DVL and the velocity calculated by SINS is used to obtain the measurement of the velocity error, and the velocity error is filtered by Kalman Filter. The attitude error, velocity error and position error estimated by Kalman filter are compensated to the attitude, velocity and position obtained by SINS to get the result of open-loop integrated navigation. (b) shows the closed-loop integrated navigation. Unlike the open-loop integrated navigation, the velocity measured by DVL and the velocity calculated by SINS is processed by

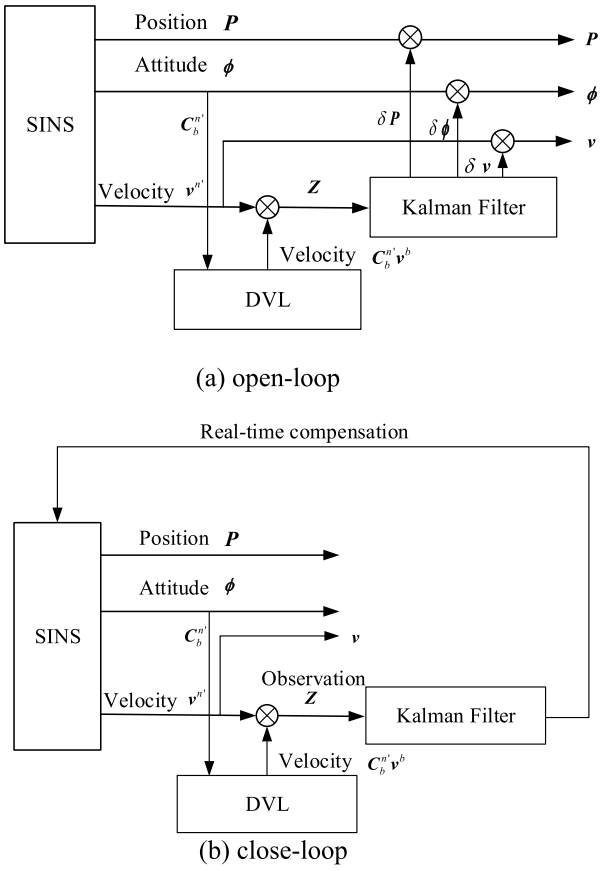

FIGURE 1. The structure of SINS/DVL.

Kalman filtering in real-time and compensated to SINS in real-time so that the attitude, velocity and position output by SINS are both passed the best estimate result. As shown in (a), if the DVL velocity needs to be converted from the b-frame to the velocity under the *n*-frame, SINS is required to provide the attitude transfer matrix. In the open-loop mode, the attitude of SINS is not compensated in time, so the error of $\boldsymbol{C}_b^n$ provided is relatively large. Therefore, we use the closed-loop integrated navigation mode.

A. ERROR MODEL OF SINS

Due to underwater vehicles' low maneuverability requirements, it is assumed that the attitude error angle in the navigation solution process is small (satisfying $\sin\theta \approx \theta$), and the initial misalignment angle is small. Therefore, establishing a linear error model can still describe the error characteristics of the SINS more accurately. Establish the linear error equation of SINS as [2]

Velocity error equation

$$\delta\dot{\boldsymbol{V}}^n = -\boldsymbol{\phi}^n \times \boldsymbol{f}^n + \delta\boldsymbol{V}^n \times \left(2\boldsymbol{\omega}_{ie}^n + \boldsymbol{\omega}_{en}^n\right) + \boldsymbol{V}^n \times \left(2\delta\boldsymbol{\omega}_{ie}^n + \delta\boldsymbol{\omega}_{en}^n\right) + \nabla^n \quad (1)$$

Position error equation

$$\delta\dot{L} = \frac{\delta V_N}{R+h} - \frac{V_N}{(R+h)^2}\delta h \quad (2)$$

$$\delta\dot{\lambda} = \frac{\sec L}{R+h}\delta V_E + \frac{V_E \sec L \tan L}{R+h}\delta L - \frac{V_E \sec L}{(R+h)^2}\delta h \quad (3)$$

Attitude error equation

$$\dot{\boldsymbol{\phi}}^n = \boldsymbol{\phi}^n \times \boldsymbol{\omega}_{in}^n + \delta\boldsymbol{\omega}_{in}^n - \boldsymbol{\varepsilon}^n \quad (4)$$

where $\delta\boldsymbol{V}^n$ denotes the velocity error, δL denotes the latitude error, $\delta\lambda$ denotes the longitude error, $\boldsymbol{\phi}^n$ denotes the attitude error angle vector, $\boldsymbol{f}^n$ is the representation of the specific force output by the accelerometer in the *n*-frame, $\boldsymbol{\omega}_{ie}^n$ is the turn rate of the Earth expressed in the *n*-frame, $\boldsymbol{\omega}_{en}^n$ is the turn rate of the *n*-frame with respect to the Earth-fixed frame, the transport rate. ∇^n is the projection of the accelerometer biased in the *n*-frame, V_N is the north velocity, V_E is the east velocity, $\boldsymbol{\varepsilon}^n$ is the projection of gyro drift under the n frame, R is the radius of the Earth, L is the local latitude and h the height above ground.

According to the SINS error equations, as mentioned above, the attitude error, velocity error, position error, gyro error, and accelerometer error are selected as the state variables. Since the altitude channel on inertial navigation system is unstable, and the measurement error of DVL up velocity is relatively large, we ignore the altitude channel. The altitude can be accurately measured by the depth gauge. The state quantity that ignores the altitude channel is selected, as shown below.

$$\boldsymbol{X}_{SINS} = \begin{bmatrix} \delta L & \delta\lambda & \delta V_E & \delta V_N & \phi_E & \phi_N & \cdots \\ \phi_U & \varepsilon_x & \varepsilon_y & \varepsilon_z & \nabla_x & \nabla_y & \nabla_z \end{bmatrix} \quad (5)$$

Establish the state equation of SINS system as

$$\dot{\boldsymbol{X}}_{SINS} = \boldsymbol{\Phi}_{SINS}\boldsymbol{X}_{SINS} + \boldsymbol{W}_{SINS} \quad (6)$$

where $\boldsymbol{\Phi}_{SINS}$ denotes the state transition matrix. $\boldsymbol{W}_{SINS}$ denotes the system noise, which is the Gaussian white noise. The definition of $\boldsymbol{\Phi}_{SINS}$ is described in [7].

B. ERROR MODEL OF DVL

According to the working principle of DVL, the measurement errors mainly include velocity offset error $\delta\boldsymbol{V}_d$, drift angle error $\delta\boldsymbol{\phi}$ and scale coefficient error δC. $\delta\boldsymbol{V}_d$ and $\delta\boldsymbol{\phi}$ are expressed by a first-order Markov process, and the corresponding error equation is shown as

$$\begin{cases} \delta\dot{\boldsymbol{V}}_d = -\beta_d\delta\boldsymbol{V}_d + \boldsymbol{w}_d \\ \delta\dot{\boldsymbol{\varphi}} = -\beta_\phi\delta\boldsymbol{\varphi} + \boldsymbol{w}_\phi \\ \delta\dot{C} = 0 \end{cases} \quad (7)$$

where β_d^{-1} and β_ϕ^{-1} are the correlation time of the first-order Markov process of $\delta\boldsymbol{V}_d$ and $\delta\boldsymbol{\phi}$ respectively; $\boldsymbol{w}_d$ and $\boldsymbol{w}_\phi$ are the Gauss white noise of $\delta\boldsymbol{V}_d$ and $\delta\boldsymbol{\phi}$ respectively, δC is a random constant.

Select velocity offset error $\delta\boldsymbol{V}_d$, drift angle error $\delta\boldsymbol{\phi}$, scale coefficient error δC as the state quantity, then the DVL state vector as

$$\boldsymbol{X}_{DVL} = \begin{bmatrix} \delta\boldsymbol{V}_d & \delta\boldsymbol{\varphi} & \delta C \end{bmatrix} \quad (8)$$

Establish the state equation of the DVL system as

$$\dot{\boldsymbol{X}}_{DVL} = \boldsymbol{\Phi}_{DVL}\boldsymbol{X}_{DVL} + \boldsymbol{W}_{DVL} \tag{9}$$

where state transition matrix $\boldsymbol{\Phi}_{DVL} = diag\left(-\beta_d, -\beta_\phi, 0\right)$, $\boldsymbol{W}_{DVL}$ is the Gauss white noise.

C. MEASUREMENT EQUATIONS OF SINS/DVL

When DVL and SINS perform integrated navigation, the difference between the velocity $\tilde{\boldsymbol{v}}^n_{SINS}$ measured by SINS and the projection of the velocity $\tilde{\boldsymbol{v}}^b_{DVL}$ measured by DVL on the n-frame is selected as the observation.

The SINS/DVL measurement equation is shown as

$$\begin{aligned}\dot{\boldsymbol{Z}}_v &= \tilde{\boldsymbol{v}}^n_{SINS} - \boldsymbol{C}^{n'}_b \boldsymbol{v}^b_{DVL} = \tilde{\boldsymbol{v}}^n_{SINS} - \boldsymbol{C}^{n'}_n \boldsymbol{C}^n_b \boldsymbol{v}^b_{DVL} \\ &= \boldsymbol{H}_v \boldsymbol{X} + \boldsymbol{V}_v\end{aligned} \tag{10}$$

where $\boldsymbol{H}_v$ is measurement matrix, $\boldsymbol{V}_v$ is measurement noise vector. Under the condition of small linear misalignment angle, $\boldsymbol{C}^{n'}_n = (\boldsymbol{I} - \boldsymbol{\phi}\times)$.

Choose east velocity error δv_E and north velocity error δv_N as observations

$$\begin{aligned}\boldsymbol{z}_v &= \begin{bmatrix}\delta v_E \\ \delta v_N\end{bmatrix} = \left[\tilde{\boldsymbol{v}}^n_{SINS} - (\boldsymbol{I} - \boldsymbol{\phi}\times)\,\boldsymbol{C}^n_b \boldsymbol{v}^b_{DVL}\right]_{2\times 3} \\ &= \left[\tilde{\boldsymbol{v}}^n_{SINS} - \boldsymbol{C}^n_b \boldsymbol{v}^b_{DVL} - \left(\boldsymbol{C}^n_b \boldsymbol{v}^b_{DVL}\right) \times \boldsymbol{\phi}\right]_{2\times 3} \\ &= \left[\tilde{\boldsymbol{v}}^n_{SINS} - \boldsymbol{v}^n_{SINS} - \left(\boldsymbol{C}^n_b \boldsymbol{v}^b_{DVL}\right) \times \boldsymbol{\phi}\right]_{2\times 3} \\ &= \left[\delta \boldsymbol{v}^n - \left(\boldsymbol{C}^n_b \boldsymbol{v}^b_{DVL}\right) \times \boldsymbol{\phi}\right]_{2\times 3}\end{aligned} \tag{11}$$

Substituting $\boldsymbol{C}^{n'}_b$ for $\boldsymbol{C}^n_b$ can get the measurement matrix $\boldsymbol{H}_v$ as

$$\boldsymbol{H}_v = \left[\boldsymbol{0}_{2\times 2}, \boldsymbol{I}_{2\times 2}, \left[-\boldsymbol{C}^{n'}_b \boldsymbol{v}^b_{DVL}\times\right]_{2\times 3}, \boldsymbol{0}_{2\times 6}\right] \tag{12}$$

where $\left[-\boldsymbol{C}^{n'}_b \boldsymbol{v}^b_{DVL}\times\right]_{2\times 3}$ denotes the first two rows of matrix $\left[-\boldsymbol{C}^{n'}_b \boldsymbol{v}^b_{DVL}\times\right]$.

III. ROBUST KALMAN FILTER

A. STANDARD KALMAN FILTER

The discrete random linear model can be described as follows

$$\begin{cases}\boldsymbol{X}_k = \boldsymbol{\Phi}_{k|k-1}\boldsymbol{X}_{k-1} + \boldsymbol{W}_{k-1} \\ \boldsymbol{Z}_k = \boldsymbol{H}_k \boldsymbol{X}_k + \boldsymbol{V}_k\end{cases} \tag{13}$$

where $\boldsymbol{X}_k$ is the state vector, $\boldsymbol{\Phi}_{k|k-1}$ is the state transition matrix, $\boldsymbol{W}_{k-1}$ is the system process noise, $\boldsymbol{Z}_k$ is the observation vector, $\boldsymbol{H}_k$ is the measurement matrix, $\boldsymbol{V}_k$ is the measurement noise vector. The system process noise $\boldsymbol{W}_{k-1}$ and the measurement noise $\boldsymbol{V}_k$ are independent Gaussian white noises with time-varying mean, and the covariance is Q and R respectively.

The Kalman filter process is as follows

$$\hat{\boldsymbol{X}}_{k|k-1} = \boldsymbol{\Phi}_{k|k-1}\hat{\boldsymbol{X}}_{k-1} \tag{14}$$

$$\boldsymbol{P}_{k|k-1} = \boldsymbol{\Phi}_{k|k-1}\boldsymbol{P}_{k-1}\boldsymbol{\Phi}^T_{k|k-1} + \hat{\boldsymbol{Q}}_{k-1} \tag{15}$$

$$\boldsymbol{K}_k = \boldsymbol{P}_{k|k-1}\boldsymbol{H}^T_k \left(\boldsymbol{H}_k \boldsymbol{P}_{k|k-1}\boldsymbol{H}^T_k + \boldsymbol{R}\right)^{-1} \tag{16}$$

$$\hat{\boldsymbol{X}}_k = \hat{\boldsymbol{X}}_{k|k-1} + \boldsymbol{K}_k\left(\boldsymbol{Z}_k - \boldsymbol{H}_k\hat{\boldsymbol{X}}_{k|k-1}\right) \tag{17}$$

$$\boldsymbol{P}_k = (\boldsymbol{I} - \boldsymbol{K}_k\boldsymbol{H}_k)\,\boldsymbol{P}_{k|k-1} \tag{18}$$

B. ROBUST KALMAN FILTER

It can be seen from the update equation (17) of $\hat{\boldsymbol{X}}_k$ that when outliers is received, $\boldsymbol{Z}_k$ will be polluted. This will lead to inaccurate $\hat{\boldsymbol{X}}_k$ estimates. To identify the outliers, the Mahalanobis distance algorithm expression considering the observation innovation at time k is as follows [28]:

$$\begin{aligned}M^2_k &= \left(\sqrt{(\boldsymbol{Z}_k - \hat{\boldsymbol{Z}}_{k|k-1})^T(\boldsymbol{P}_{ee,k|k-1})^{-1}(\boldsymbol{Z}_k - \hat{\boldsymbol{Z}}_{k|k-1})}\right)^2 \\ &= \boldsymbol{\mu}^T_k(\boldsymbol{P}_{zz,k|k-1} + \boldsymbol{R})^{-1}\boldsymbol{\mu}_k\end{aligned} \tag{19}$$

where M_k is the Mahalanobis distance, $\boldsymbol{P}_{zz,k|k-1} = \boldsymbol{H}_k\boldsymbol{P}_{k|k-1}\boldsymbol{H}^T_k$, $\boldsymbol{Z}_k$ is the value of the observation.

To further realize the robustness of KF, an expansion factor λ_k is introduced. When the innovation is abnormal, the measurement noise covariance is expanded; on the contrary, when the innovation is normal, $\lambda_k = 1$.

If its Mahalanobis distance satisfies $M^2_k > \chi^2_{n,\alpha}$, $\tilde{\boldsymbol{z}}_k$ will be marked as an abnormal observation. Simultaneously, an expansion factor λ_k is introduced to expand the measurement noise covariance matrix $\boldsymbol{R}$, namely

$$\tilde{\boldsymbol{R}}_k = \lambda_k \boldsymbol{R} \tag{20}$$

Substituting (20) into (19) can get:

$$\begin{aligned}\vartheta_k &= M^2_k = \boldsymbol{\mu}^T_k(\tilde{\boldsymbol{P}}_{\hat{\boldsymbol{z}}_{k|k-1}})^{-1}\boldsymbol{\mu}_k \\ &= \boldsymbol{\mu}^T_k(\boldsymbol{P}_{zz,k|k-1} + \tilde{\boldsymbol{R}}_k)^{-1}\boldsymbol{\mu}_k \\ &= \boldsymbol{\mu}^T_k(\boldsymbol{P}_{zz,k|k-1} + \lambda_k\boldsymbol{R})^{-1}\boldsymbol{\mu}_k = \chi^2_{n,\alpha}\end{aligned} \tag{21}$$

(21) can be transformed into a nonlinear problem for solving λ_k, as shown in (22).

$$f(\lambda_k) = \boldsymbol{\mu}^T_k(\boldsymbol{P}_{zz,k|k-1} + \lambda_k\hat{\boldsymbol{R}}_k)^{-1}\boldsymbol{\mu}_k - \chi^2_{n,\alpha} \tag{22}$$

where λ_k can be solved by the Newton iteration method. Therefore, the relationship between $\lambda_k(i+1)$ and $\lambda_k(i)$ can be expressed as:

$$\lambda_k(i+1) = \lambda_k(i) + \frac{\vartheta_k(i) - \chi^2_{n,\alpha}}{\boldsymbol{\mu}^T_k(\tilde{\boldsymbol{P}}_{\hat{\boldsymbol{Z}}_{k|k-1}}(i))^{-1}\hat{\boldsymbol{R}}_k(\tilde{\boldsymbol{P}}_{\hat{\boldsymbol{Z}}_{k|k-1}}(i))^{-1}\boldsymbol{\mu}_k} \tag{23}$$

where $\tilde{\boldsymbol{P}}_{\hat{\boldsymbol{z}}_{k|k-1}}(i) = \boldsymbol{P}_{zz,k|k-1} + \lambda_k(i)\boldsymbol{R}$, and the initial value of $\lambda_k(i)$ is $\lambda_k(0) = 1$. When the evaluation index meets $\vartheta_k(i) \le \chi^2_{n,\alpha}$, the iteration is terminated. In this paper, the probability parameter α is set be 0.99, this to say the efficiency of robust filtering method is 99%, and the value of 2-degree-of-freedom Chi-square distribution $\chi^2_{2,0.99}$ is 9.2 [28].

IV. DEEP LEARNING MODEL

A. RECURRENT NEURAL NETWORK

Recurrent Neural Network (RNN) is a neural network that can process time-series information. RNN was first applied to the field of natural grammar processing, and with the promotion of deep learning, it was applied to the field of load forecasting of power systems. The structure consists of an input layer, a hidden layer, and an output layer in the traditional neural network model. The hidden layer from the input layer to the output layer is unidirectional, and the nodes between the hidden layers are not connected. Normal neural networks usually cannot be used to process sequence data. The sequence output by the RNN at the current moment will be associated with the sequence output at the previous moment; that is, the network will remember the previous sequence and apply it to the current sequence. In RNN, the nodes between hidden layers are no longer unconnected but connected, and the input of the hidden layer includes the output of the input layer and the output of the previously hidden layer [32], [33].

There are many types of RNNs. The most basic recurrent neural network includes an input layer, a hidden layer, and an output layer, as shown in Fig. 2.

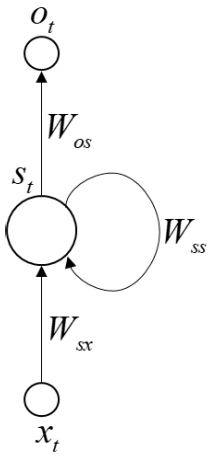

FIGURE 2. The basic structure of RNN.

In Fig. 2. x_t is the input vector, which is the value of the input layer, S_t is the value of the hidden layer. W_{sx} is the weight matrix from the input layer to the hidden layer, O_t is the value of the output layer. W_{os} is the weight from the hidden layer to the output layer matrix. The value s of the hidden layer of the cyclic neural network depends not only on the current input x, but also on the value s of the last hidden layer. The weight matrix W_{ss} is the last value of the hidden layer as the weight of this input. If the W_{ss} circle is removed, RNN becomes the most common fully connected neural network.

B. NARX

Nonlinear AutoRegressive with eXogenous input (NARX) with external output is another type of neural network suitable for nonlinear systems and time series prediction. NARX

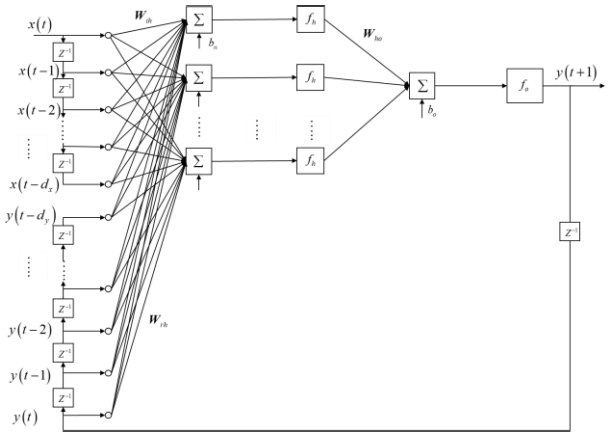

FIGURE 3. The basic structure of NARX.

network is a dynamic neural network, which contains multiple layers of cyclic feedback. Fig. 3 shows the structure of NARX [34], [35].

According to the Fig. 3, the relationship between the input sequence $\boldsymbol{x}(t)$ and output sequence $\boldsymbol{y}(t)$ of NARX can be obtained as shown in the formula

$$y(t+1) = f\left[x(t), \cdots, x(t-d_x); y(t), \cdots, y\left(t-d_y\right)\right] \tag{24}$$

where d_x and d_y are input delay and output delay respectively.

Substituting the NARX model parameters into (24) can get (25).

$$y(t+1) = f_o\left[b_o + \sum_{h=1}^{Nh} w_{ho} \cdot f_h\left(b_h + \sum_{i=0}^{d_x} w_{ih} x(t-i) + \sum_{r=0}^{d_y} w_{rh} y(n-r)\right)\right] \tag{25}$$

where w_{ih}, w_{rh} and w_{ho} are the weights, where $i = 1, 2, \cdots, d_x$; $r = 1, 2, \cdots, d_y$; $h = 1, 2, \cdots, Nh$, $f_h(\cdot)$ and $f_o(\cdot)$ are the activation functions of the hidden layer and the output layer, respectively. b_h and b_o are the bias of the hidden unit and output unit respectively.

C. NARX MODEL OF INTEGRATED NAVIGATION SYSTEM

According to the analysis of [21], the navigation parameters are coupled with each other, and the sensor bias is closely related to the external environment and motion state. SINS error changes have specific laws, and the navigation status error has a strong correlation with historical information. This is consistent with the characteristics of the time series forecasting model, so we use the time series forecasting model to predict the output of DVL. The inherent error model of the inertial device can be obtained by training a neural network. We propose a prediction model based on the NARX network. When the DVL output velocity information is normal, the information obtained by the SINS solution and the DVL output information can be used to train the model.

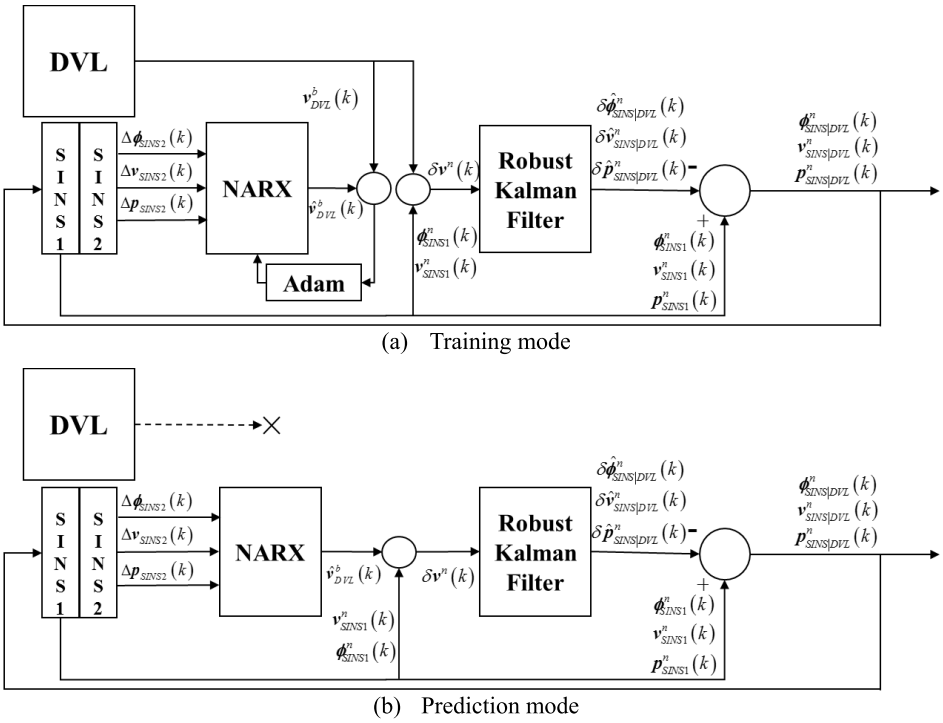

FIGURE 4. The Structure of NARX.

The integrated navigation model optimized by NARX is shown in Fig. 4. Among them, Fig. 4. (a) is the training mode of the model when DVL is available. We use a set of inertial measurement units (IMU) measured inertial data for a two-channel solution. In other words, the SINS outputs two sets of independent data through the solution of two independent channels. SINS channel 1 is a closed-loop integrated navigation solution, which uses the velocity measured by DVL and the navigation information solved by channel 1 to perform RKF in real-time, and real-time feedback compensation to channel 1. SINS channel 2 is a pure inertial solution. After the initial navigation information is given, the solution depends entirely on the IMU's inertial data. In the training mode, the input sequence of the NARX network selects the attitude increment $\Delta\boldsymbol{\phi}$, position increment $\Delta\boldsymbol{p}$ and velocity increment Δv obtained by the SINS channel 2 solution. The input sequence is $\left[\Delta\boldsymbol{\phi}_k \ \Delta\boldsymbol{p}_k \ \Delta\boldsymbol{v}_k\right]$. The target sequence of the NARX network is the velocity under the *b*-frame output by DVL. We use Adam optimization algorithm [36] to train the model.

Fig. 4 (b) shows the prediction mode when DVL is interrupted. The DVL output is predicted through the trained NARX network. When predicting, the input of NARX is the attitude increment $\Delta\boldsymbol{\phi}$, position increment $\Delta\boldsymbol{p}$ and velocity increment $\Delta\boldsymbol{v}$ obtained by SINS channel 2 pure inertia solution. Since it has been fully trained, the velocity of DVL output, that is, the AUV's velocity in the *b*-frame, can be predicted by the NARX network. Using the predicted velocity, RKF can be performed with the velocity obtained by the closed-loop integrated navigation of SINS channel 1 to obtain the estimation error and correct the navigation information obtained by SINS channel 1. At the same time, real-time feedback to channel 1 navigation information and perform the next solution.

TABLE 1. Hyperparameters.

Number of hidden layers	1
Node per layer	9-100-3
Input delay	0
Output delay	1
Number of epochs	1000
Initial learning rate	0.05
Learn rate drop period	1
Learn rate drop factor	0.98

TABLE 2. Instruments and specifications.

	Gyroscope	Accelerator	DVL
Update Rate	200Hz	200Hz	1Hz
Constant Drift	<0.02°/h	$<5 \times 10^{-5}$g	/
Accuracy Level	/	/	0.5%V±0.5cm/s

The hyperparameters used in this model are shown in TABLE 1.

V. EXPERIMENT STUDYS

The experimental data is collected through a set of the ship-mounted experimental system, including SINS and DVL, and a GPS receiver with a single antenna installed. The specifications of the IMU and DVL used in the experimental system are shown in Table 2.

Using the velocity and position information received by the GPS receiver, integrated with the data output by SINS, can generate reference attitude, velocity and position, which

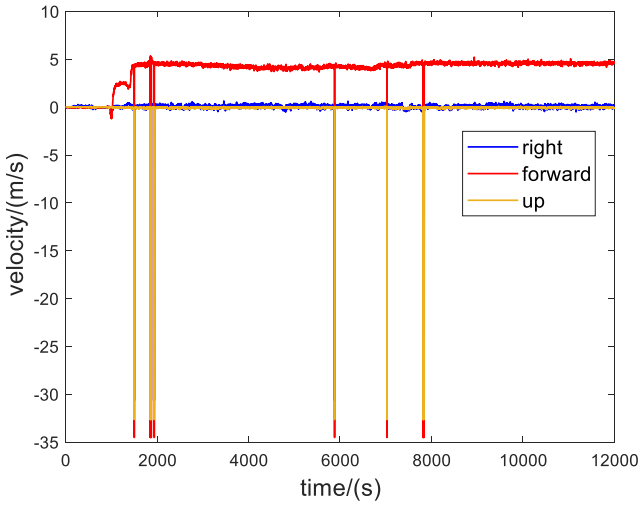

FIGURE 5. The output of DVL.

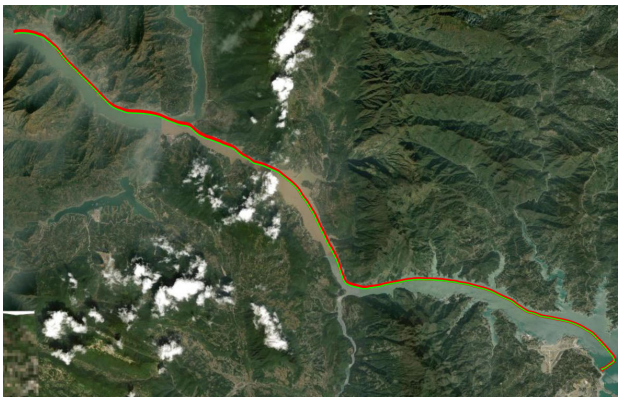

FIGURE 6. Experimental trajectory.

can be used as the benchmark for this experiment. The ship-mounted experimental was carried out in the Yangtze River. The experimental process was designed as follows: when the experimental system is turned on, the experimental ship remains moored for about 15 minutes; then, the experimental ship sails out and moves for about 6 hours.

A section of 9000s ship-mounted measured data is selected for the semi-physical simulation experiment verification of the model proposed in this paper. The selected data includes the gyroscope and accelerometer's raw data, the velocity data output by the DVL, the corresponding attitude reference, velocity reference and position reference. The velocity data output by DVL as shown in Fig. 5. When using the data output by DVL, due to the misalignment angle between the DVL and the SINS mounting frame, it needs to be corrected. The data used in this semi-physical simulation experiment has been corrected.

Perform integrated navigation calculation on SINS and DVL data of 9000s, and the obtained trajectory is shown as the green line in Fig. 6. When DVL does not fail, this track is the normal integrated navigation track. Simultaneously, the reference trajectory obtained by SINS/GPS integrated navigation is shown as the red line in Fig. 6.

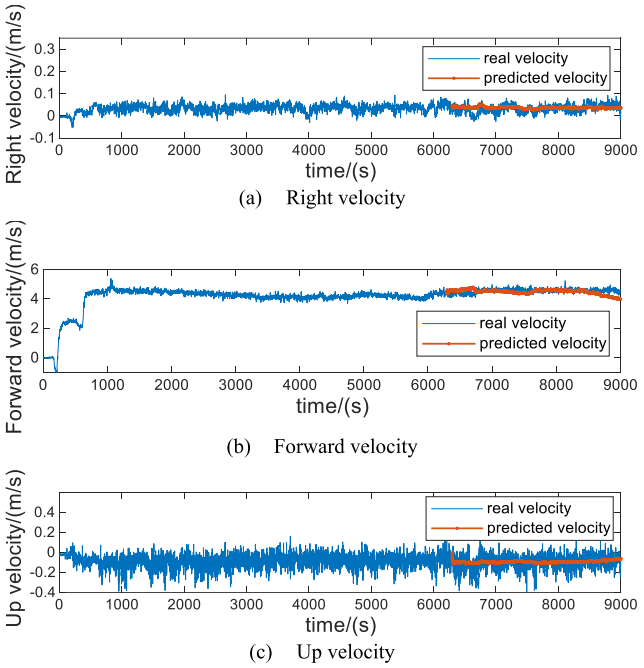

FIGURE 7. Prediction of v^b_{DVL}.

Use the first 70% of the 9000s ship-mounted measured data as the training set, fit the model, and adjust the network weight. The last 30% is used as a test set to evaluate the model's generalization ability and confirm the actual predictive ability of the network. In other words, use the first 70% of the SINS output and DVL output to train the deep learning model. In the last 30% of the data, the DVL interruption is simulated, and the DVL output is predicted through the deep learning model through the SINS output data and integrated navigation is performed.

The DVL output is shown in Fig. 5, and you can see that there are multiple outliers with an amplitude of -35m/s. This shows that DVL is susceptible to outliers when working in underwater integrated navigation.

We consider two different situations to verify the effectiveness of the proposed algorithm.

(1) Preprocess the DVL data first, and eliminate the outliers of the DVL data. Only assume that the last 30% are DVL interruptions to verify the NARX predictive model's effectiveness.

(2) Do not preprocess the outliers of the DVL data, and assume that the last 30% are DVL interrupts to verify the effectiveness of the proposed NARX-RKF.

A. PERFORMANCE COMPARISON WHEN DVL MALFUNCTIONS

The experimental results of situation 1, as shown in Figs. 7-12. In this experiment, we eliminate outliers in advance and only verified the predictive ability of the NARX model when DVL is interrupted. Fig. 7 shows the DVL output predicted by the NARX model when the DVL interrupt is simulated. In the figure, blue is the real velocity of DVL output. However, at 6301 seconds, we interrupt DVL. That is

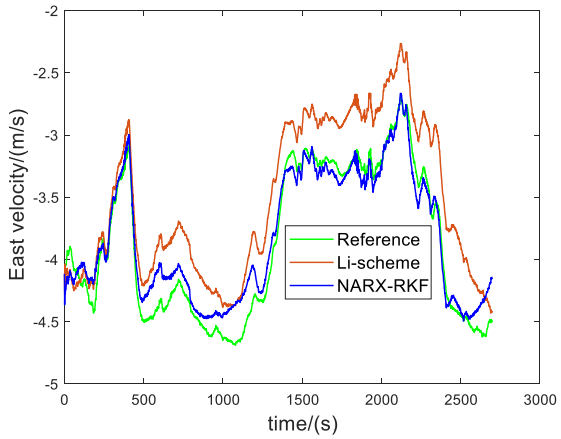

(a) East velocity

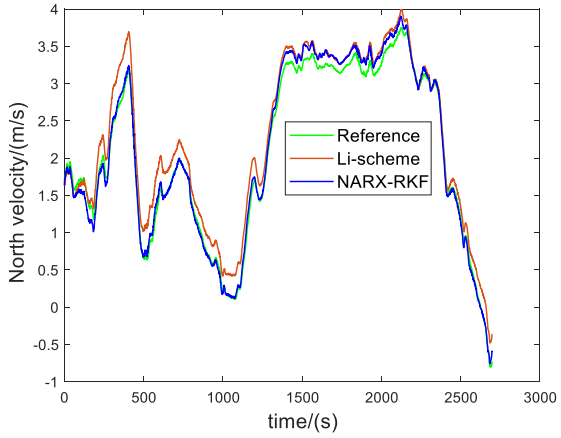

(b) North velocity

FIGURE 8. Comparison of prediction effect of v^n_{DVL}.

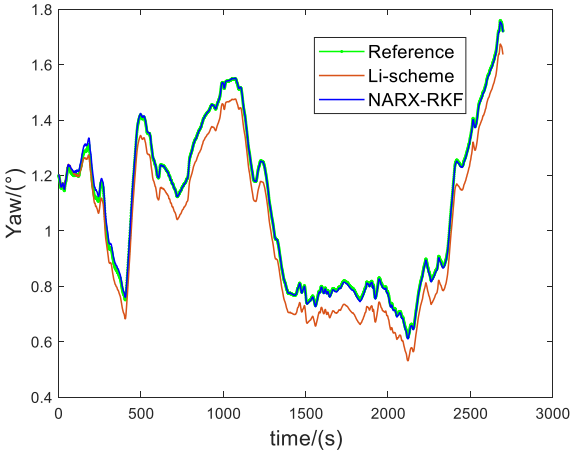

FIGURE 9. Comparison of prediction effect of Yaw.

to say, we assume that data from 6301 seconds to 9000 seconds cannot be obtained through DVL. The red curve is the DVL output predicted by the NARX model. The next step of integrated navigation can be carried out by the predicted velocity.

Using the predicted $\hat{\boldsymbol{v}}^b_{DVL}$ and the attitude obtained through the closed-loop integrated navigation, $\hat{\boldsymbol{v}}^b_{DVL}$ can be converted into $\hat{\boldsymbol{v}}^n_{DVL}$. Fig. 8 is the East velocity and North velocity of

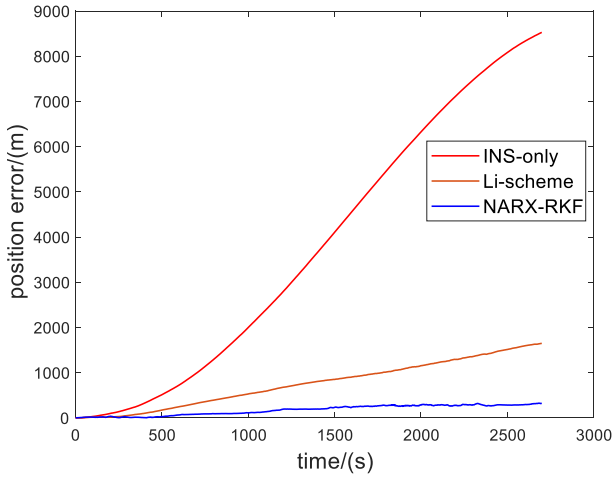

FIGURE 10. Prediction of position error relative to SINS/DVL reference position.

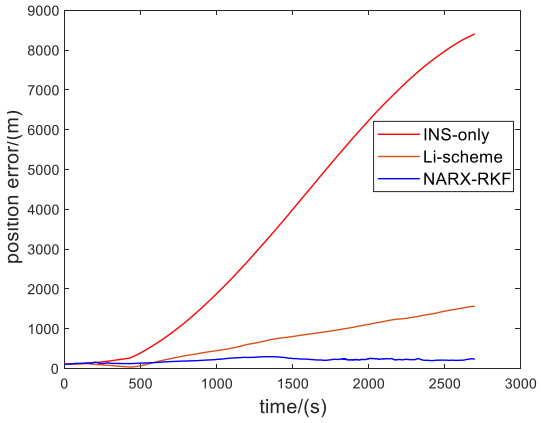

FIGURE 11. Prediction of position error relative to SINS/GPS reference position.

$\boldsymbol{v}^n$. The green curve is the reference velocity obtained by using SINS/GPS integrated navigation, and the blue curve is the velocity obtained by the model proposed in this paper. The Li-scheme curve is the method proposed in the [22], we are using the same deep learning model, but the structure of the integrated navigation algorithm is different, so we make a comparison. It can be seen from the figure that the method proposed in this paper has a higher prediction accuracy for velocity than the method in [22].

Fig. 9 is the yaw obtained by using the predicted velocity for integrated navigation solution. It can be seen that the attitude obtained by the NARX-RKF method is much more accurate than the method in [22], and it is very close to the reference value.

In the last 2700s, if the DVL works normally and the position obtained by the SINS/DVL integrated navigation is used as the reference value, a comparison can be made. The position calculated by pure inertia, the position predicted by the method [22], and the position predicted by NARX-RKF proposed in this paper are compared with the reference value. The position error obtained is shown in Fig. 10. In practice, if the AUV has no position observation, when DVL is

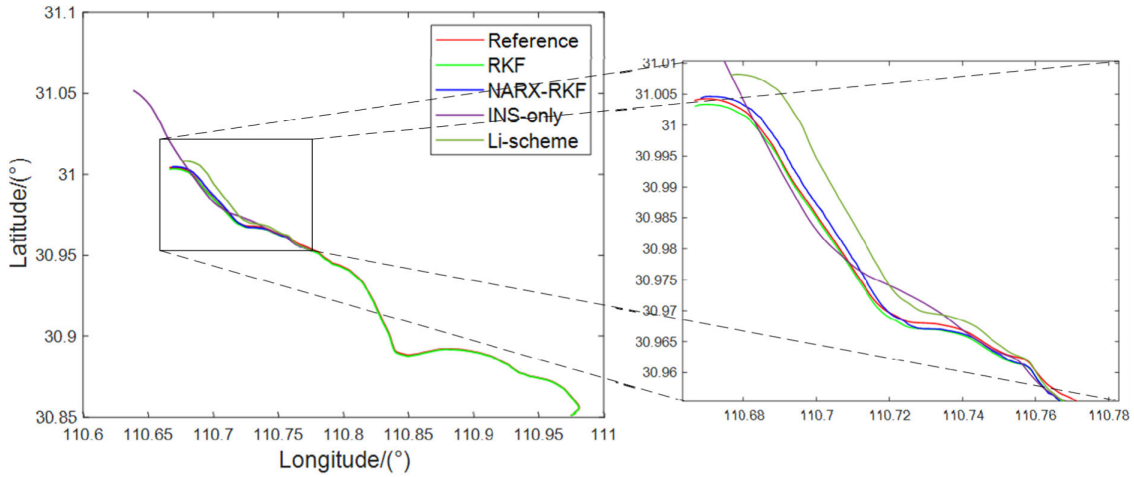

FIGURE 12. Trajectories obtained by integrated navigation of different methods.

interrupted, only pure inertial calculation can be performed. The error of pure inertial solution accumulates rapidly over time, as shown by the red curve in Fig. 10. Using NARX-RKF to predict the carrier velocity output by DVL and then performing integrated navigation, the error is greatly reduced compared to the pure inertial solution. Compared with pure inertial solution, NARX-RKF improves its position accuracy by 96.27%. Compared with the model in [22], its position accuracy is improved by 80.70%.

In fact, when there is no position observation, the positioning error of SINS/DVL integrated navigation cannot be eliminated, that is, the positioning error of SINS/DVL integrated navigation is not appreciable. We believe that the GPS accuracy is high enough, the reference position obtained by SINS/GPS integrated navigation is the real position, and the position error as shown in the Fig. 11. It can also be seen that the positioning accuracy of NARX-RKF is greatly improved compared to the pure inertial solution and the model [22].

Fig. 12. is the trajectory comparison diagram of the experiment, in which the RKF curve represents the integrated navigation result when the DVL is always normal, and the Li-scheme is the method proposed in the [22]. It can be seen from the figure that the trajectory of NARX-RKF is very close to the reference trajectory. The effect of Li-scheme is worse than NARX-RKF.

B. DVL POLLUTED BY OUTLIERS AND INTERRUPTION

Due to the complexity of the underwater environment, we have to consider the outliers pollution when DVL is affected by complex conditions. In order to prove the necessity of improving the model's robustness, the DVL output of the following experiment did not preprocess the outliers, but only corrected the constant error matrix. This represents the output of DVL's real underwater environment.

The experimental results are shown in Figs. 13-15. Fig. 13 shows the prediction of DVL output using NARX-RKF.

Two frameworks of NARX-KF and NARX-RKF were used for prediction. The structure and parameters of the NARX

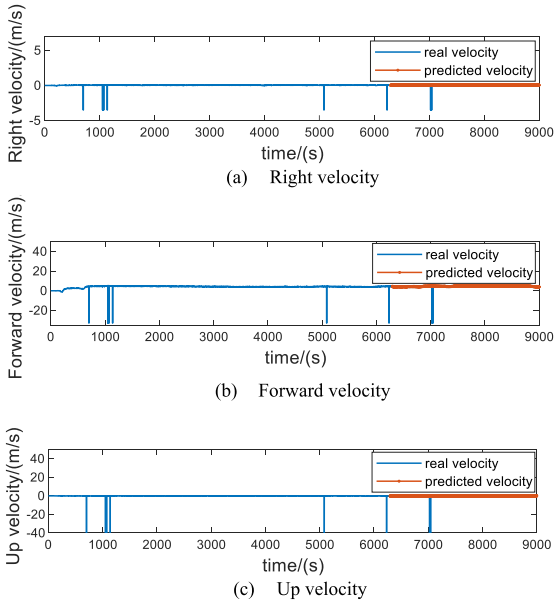

FIGURE 13. Prediction of v^b_{DVL} under outlier pollution.

network part of the two frameworks are exactly the same, only the integrated navigation filter part is different.

Fig. 14 shows the velocity predicted by NARX-KF and NARX-RKF, respectively. It can be seen from the figure that the two models have similar velocity prediction capabilities. It shows that even if the training data is contaminated by outliers, it has little effect on the prediction results. Shows that NARX is robust.

Fig. 15. is a comparison diagram of the integrated navigation results. In the figure, the red curve is the reference position. The KF and RKF curves are the results of normal navigation using different algorithms when DVL is not interrupted. It can be seen that the KF algorithm without robustness diverges when it is polluted by outliers. The NARX-KF curve and NARX-RKF curve are the positions obtained by using NARX to predict the velocity of *b*-frame and using the KF and RKF integrated navigation respectively after 6301

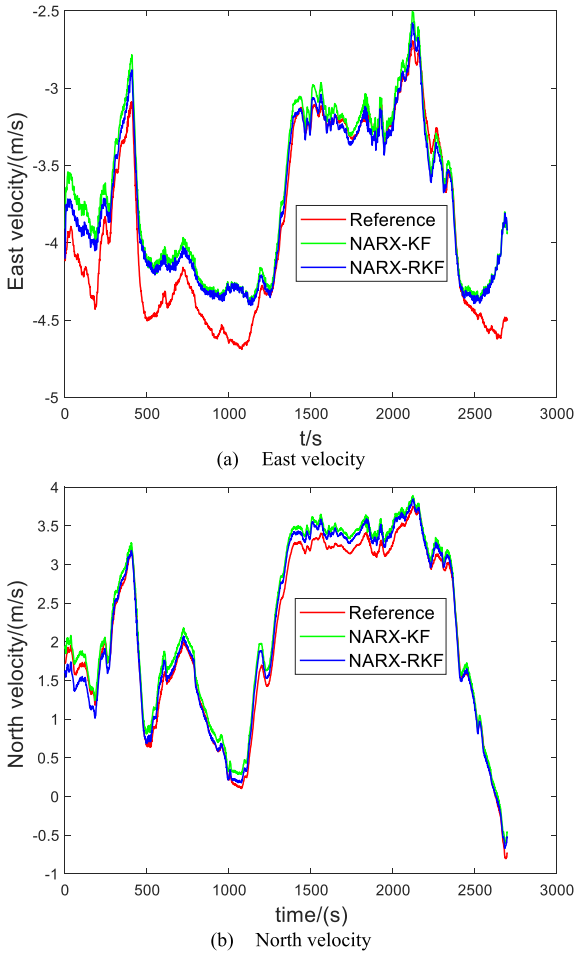

FIGURE 14. The velocity predicted by different methods.

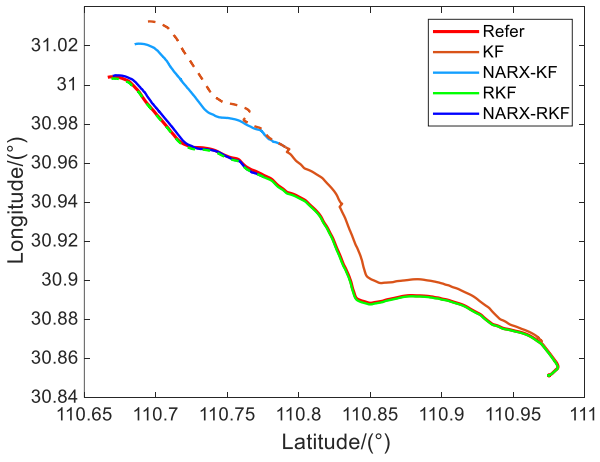

FIGURE 15. Trajectories of different methods.

seconds to simulate the DVL interruption. It can be seen that the NARX-KF position divergence is more serious due to outliers. NARX-RKF uses the Mahalanobis distance algorithm to eliminate outliers, so the integrated navigation effect is better.

Because the neural network initializes parameters with random numbers, and then continuously learns to modify the parameters of random initialization. In order to verify the universality of NARX-RKF and prevent the contingency of a single experiment, we introduce Monte Carlo experiments. In each Monte Carlo experiment, a quantitative error analysis is performed on the two models, and the root mean square error (RMSE) is used as the metric here.

TABLE 3. ARMSE comparison.

	1-6300s DVL available		6301-9000s DVL is interrupted	
	Velocity error(m/s)	Position error/(m)	Velocity error(m/s)	Position error/(m)
NARX-KF	0.5242	1249.5586	0.2931	1908.7323
NARX-RKF	0.1007	52.1428	0.2340	291.3621

$$RMSE = \sqrt{\frac{1}{n}\sum_{t=1}^{n}\left(\hat{y}_t - y_t\right)} \tag{26}$$

Then perform 50 Monte Carlo experiments and calculate the Average RMSE (ARMSE) of the 50 experiments.

$$ARMSE = \frac{1}{50}\sum_{k=1}^{50} RMSE_k \tag{27}$$

It can be concluded from the above experimental results that if NARX-KF is polluted by outliers during the model training phase, it will have a great impact on the integrated navigation results. Compared with NARX-KF, NARX-RKF has stronger robustness and is more suitable for integrated navigation applications in complex underwater environments.

VI. CONCUSION

This paper proposes an algorithm for AUV integrated navigation, called NARX-RKF, to improve the navigation accuracy of the SINS/DVL integrated navigation system when DVL is polluted by outliers and DVL is interrupted. NARX-RKF includes a DVL failure prediction output module based on NARX model and an RKF integrated navigation loop. NARX can use inertial navigation output information to predict the output when DVL is interrupted, and use RKF for integrated navigation. We verify the proposed algorithm's effectiveness through the data collected by the ship-mounted experimental system and through comparison with some related work.

ACKNOWLEDGMENT

The authors sincerely thank Bing Zhu from the Beijing Institute of Tracking and Telecommunication Technology for his help and suggestions.

REFERENCES

[1] J. Xu, "Analysis on underwater PNT system and key technologies," *Navigat. Positiong Timing*, vol. 4, no. 1, pp. 1–6, 2017.
[2] D. Titterton, J. L. Weston, and J. Weston, *Strapdown Inertial Navigation Technology*, vol. 17. Edison, NJ, USA: IET, 2004.
[3] H. Rice, S. Kelmenson, and L. Mendelsohn, "Geophysical navigation technologies and applications," in *Proc. PLANS . Position Location Navigat. Symp.*, Apr. 2004, pp. 618–624.

[4] Z. Deng, Y. Ge, W. Guan, and K. Han, "Underwater map-matching aided inertial navigation system based on multi-geophysical information," *Frontiers Electr. Electron. Eng. China*, vol. 5, no. 4, pp. 496–500, Dec. 2010.
[5] S. Guiguo, Z. Jun, and G. Zhilei, "An approach to autonomous navigation using matching of geophysical features," *J. Northwestern Polytech. Univ.*, vol. 28, no. 1, pp. 18–22, 2010.
[6] W. Li, W. Wu, J. Wang, and L. Lu, "A fast SINS initial alignment scheme for underwater vehicle applications," *J. Navigat.*, vol. 66, no. 2, pp. 181–198, Mar. 2013.
[7] B. Zhu and H. He, "Integrated navigation for Doppler velocity log aided strapdown inertial navigation system based on robust IMM algorithm," *Optik*, vol. 217, Sep. 2020, Art. no. 164871.
[8] B. Zhu, G. Chang, H. He, and J. Xu, "Robust information fusion method in SINS/DVL/AST underwater integrated navigation," *J. Nat. Univ. Defense Technol.*, vol. 42, no. 5, pp. 107–114, 2020.
[9] R. E. Kalman, "A new approach to linear filtering and prediction problems," *J. Basic Eng.*, vol. 82, no. 1, pp. 35–45, Mar. 1960.
[10] T. R. Penn, "All source sensor integration using an extended Kalman filter," M.S. thesis, AFIT, Air Univ., Dayton, OH, USA, 2012.
[11] F. Li, J. Xu, and H. He, "Backtracking velocity denoising based autonomous in-motion initial alignment," *IEEE Access*, vol. 6, pp. 67144–67155, 2018.
[12] X. Xu, Y. Pan, and H. Zou, "SINS/DVL integrated navigation system based on adaptive filering," *J. Huazhong Univ. Sci. Tech. (Natural Sci. Ed.)*, vol. 43, no. 3, pp. 95–99, 2015.
[13] A. Mirabadi, "Fault detection and isolation in multisensor train navigation systems," in *Proc. UKACC Int. Conf. Control (CONTROL)*, 1998, pp. 969–974.
[14] C. Chen, P. Zhao, C. Lu, W. Wang, A. Markham, and N. Trigoni, "Deep learning based pedestrian inertial navigation: Methods, dataset and on-device inference," *IEEE Internet Things J.*, vol. 7, no. 5, pp. 4431–4441, May 2020.
[15] M.-D. Zhang, H.-F. Dai, B.-Q. Hu, and Q. Chen, "Robust adaptive UKF based on SVR for inertial based integrated navigation," *Defence Technol.*, vol. 16, no. 4, pp. 846–855, Aug. 2020.
[16] E. S. Abdolkarimi, G. Abaei, and M. R. Mosavi, "A wavelet-extreme learning machine for low-cost INS/GPS navigation system in high-speed applications," *GPS Solutions*, vol. 22, no. 1, p. 15, Jan. 2018.
[17] X. Chen, C. Shen, W.-B. Zhang, M. Tomizuka, Y. Xu, and K. Chiu, "Novel hybrid of strong tracking Kalman filter and wavelet neural network for GPS/INS during GPS outages," *Measurement*, vol. 46, no. 10, pp. 3847–3854, Dec. 2013.
[18] S. Adusumilli, D. Bhatt, H. Wang, P. Bhattacharya, and V. Devabhaktuni, "A low-cost INS/GPS integration methodology based on random forest regression," *Expert Syst. Appl.*, vol. 40, no. 11, pp. 4653–4659, Sep. 2013.
[19] J. Li, N. Song, G. Yang, M. Li, and Q. Cai, "Improving positioning accuracy of vehicular navigation system during GPS outages utilizing ensemble learning algorithm," *Inf. Fusion*, vol. 35, pp. 1–10, May 2017.
[20] K.-W. Chiang, Y.-W. Huang, and X. Niu, "Rapid and accurate INS alignment for land applications," *Surv. Rev.*, vol. 42, no. 317, pp. 279–291, Jul. 2013.
[21] H.-F. Dai, H.-W. Bian, R.-Y. Wang, and H. Ma, "An INS/GNSS integrated navigation in GNSS denied environment using recurrent neural network," *Defence Technol.*, vol. 16, no. 2, pp. 334–340, Apr. 2020.
[22] W. Li, M. Chen, C. Zhang, L. Zhang, and R. Chen, "A novel neural network-based SINS/DVL integrated navigation approach to deal with DVL malfunction for underwater vehicles," *Math. Problems Eng.*, vol. 2020, pp. 1–14, Jul. 2020.
[23] D.-C. Chang and W.-R. Wu, "Feedback median filter for robust preprocessing of glint noise," *IEEE Trans. Aerosp. Electron. Syst.*, vol. 36, no. 4, pp. 1026–1035, Oct. 2000.
[24] T. Cipra and R. Romera, "Robust Kalman filter and its application in time series analysis," *Kybernetika*, vol. 27, no. 6, pp. 481–494, 1991.
[25] C. Boncelet and B. Dickinson, "An approach to robust Kalman filtering," in *Proc. 22nd IEEE Conf. Decis. Control*, Dec. 1983, pp. 304–305.
[26] C. D. Karlgaard and H. Schaub, "Huber-based divided difference filtering," *J. Guid., Control, Dyn.*, vol. 30, no. 3, pp. 885–891, May 2007.
[27] L. Chang, B. Hu, G. Chang, and A. Li, "Huber-based novel robust unscented Kalman filter," *IET Sci. Meas. Technol.*, vol. 6, no. 6, pp. 502–509, Nov. 2012.
[28] G. Chang, "Robust Kalman filtering based on mahalanobis distance as outlier judging criterion," *J. Geodesy*, vol. 88, no. 4, pp. 391–401, Apr. 2014.
[29] F. El-Hawary and Y. Jing, "Robust regression-based EKF for tracking underwater targets," *IEEE J. Ocean. Eng.*, vol. 20, no. 1, pp. 31–41, Jan. 1995.
[30] Y. Huang and Y. Zhang, "Robust student's t-based stochastic cubature filter for nonlinear systems with heavy-tailed process and measurement noises," *IEEE Access*, vol. 5, pp. 7964–7974, 2017.
[31] G. Chang and M. Liu, "M-estimator-based robust Kalman filter for systems with process modeling errors and rank deficient measurement models," *Nonlinear Dyn.*, vol. 80, no. 3, pp. 1431–1449, May 2015.
[32] A. Graves, "Generating sequences with recurrent neural networks," 2013, *arXiv:1308.0850*. [Online]. Available: http://arxiv.org/abs/1308.0850
[33] L. R. Medsker and L. C. Jain, "Recurrent neural networks," *Des. Appl.*, vol. 5, 2001.
[34] E. Diaconescu, "The use of NARX neural networks to predict chaotic time series," *WSEAS Trans. Comput. Res.*, vol. 3, no. 3, pp. 182–191, Mar. 2008.
[35] T. Lin, B. G. Horne, P. Tino, and C. L. Giles, "Learning long-term dependencies in NARX recurrent neural networks," *IEEE Trans. Neural Netw.*, vol. 7, no. 6, pp. 1329–1338, Nov. 1996.
[36] D. P. Kingma and J. Ba, "Adam: A method for stochastic optimization," 2014, *arXiv:1412.6980*. [Online]. Available: http://arxiv.org/abs/1412.6980

DING LI received the B.Eng. degree from the University of South China, Hengyang, China, in 2019. He is currently pursuing the M.Eng. degree with the College of Electrical Engineering, Naval university of Engineering, Wuhan, China. His research interests include inertial navigation systems, data fusion, and underwater integrated navigation.

JIANGNING XU received the B.Sc. degree from Northwestern Polytechnical University, Xi'an, China, in 1986, the M.Sc. degree from the Naval University of Engineering, Wuhan, China, in 1989, and the Ph.D. degree in navigation engineering from Southeast University, Nanjing, China, in 2014. He is currently a Professor with the Naval University of Engineering. His current research interests include position navigation and timing, inertial navigation systems, and integrated navigation theory.

HONGYANG HE received the B.Sc. degree in mechanical design and automation from the School of Marine Science and Technology, Northwestern Polytechnical University, Xi'an, China, in 2011, and the M.Sc. and Ph.D. degrees in navigation engineering from the Naval University of Engineering, Wuhan, China, in 2013 and 2016, respectively. He is currently working as an Assistant Professor with the Naval University of Engineering. His research interests include the inertial navigation systems and position navigation and timing.

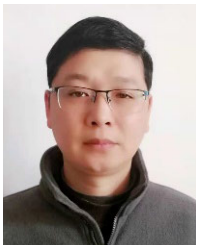

MIAO WU received the B.Sc. degree in navigation engineering and the M.Sc. degree in communication engineering from the Navel University of Engineering, Wuhan, China, in 2000 and 2006, respectively, and the Ph.D. degree in geodesy from the University of Chinese Academy of Sciences, in 2013. He is currently an Associate Professor with the Naval University of Engineering. His current research interests include position navigation and timing, radio navigation systems, and signal processing.